PCCP

Chemical dynamics of the protonated water trimer analyzed by transition path sampling

Philip L. Geissler, Christoph Dellago and David Chandler*

Department of Chemistry, University of California, Berkeley, CA 94720, USA

Received 12th November 1998, Accepted 22nd December 1998

Using transition path sampling, we have identified the two most important classes of reaction pathways and computed microcanonical rate constants for proton transfer in a model of $(H_2O)_3H^+$. The path sampling simulations visit the pathways in correct proportion despite the presence of a high potential energy barrier separating the two transition state regions. In both classes of pathways, transfer is driven by rearrangement of the oxygen ring rather than by distortion of chemical bonds. The potential experienced by the transferring proton is monostable throughout the transition, so that proton tunneling is not expected to play a large role in these dynamics. Transient times to traverse either transition state region are typically of the order of 0.1 ps. In contrast, proton residence times are 15 or more orders of magnitude longer for energies below the dissociation threshold. The computed residence times (or rate constants) vary by 25 orders of magnitude over the range of energies we have considered. Over this range, the energy scaling predicted by classical RRKM theory agrees well with that found from the computed rates.

I Introduction

Proton transfer in aqueous environments has attracted considerable theoretical attention due to its fundamental importance in chemical and biological systems. Understanding the microscopic dynamics of proton transfer, however, has proved computationally challenging because of the wide ranges of energy scales and time scales involved. While approaches such as Car–Parrinello molecular dynamics[1] allow *ab initio* treatment of electronic and interatomic energies along finite-temperature trajectories, the computational cost of these approaches encourages the use of empirical models. These physically motivated but approximate models, which range from effective interatomic potentials[2] to few quantum state descriptions,[3,4] circumvent the problem of disparate energy scales by treating electronic degrees of freedom implicitly. The problem of disparate time scales, however, remains a serious difficulty in most proton transfer processes of chemical interest. In bulk water, microscopic transport of an excess proton occurs with a characteristic time of a few picoseconds, a time scale just within the reach of *ab initio* molecular dynamics.[5,6] Autodissociation of a water molecule in bulk water and proton transfer in small water clusters involve residence times significantly longer than accessible time scales in straightforward simulations.

In principle, transition path sampling[7–9] provides the means to overcome this problem of disparate time scales. To examine the suitability in practice, the present work uses transition path sampling[7] to determine the rate and mechanisms of proton transfer in an empirical model of $(H_2O)_3H^+$. The particular model considered in this paper is the polarizable and dissociable model of Stillinger and David.[2] Preliminary results indicate that the findings of the current paper are consistent with those derived from transition path sampling and *ab initio* molecular dynamics applied to the same system.[10]

The transition path sampling method, reviewed in Section II, harvests an ensemble of deterministic trajectories connecting two stable states, so that the comparatively long times the system spends between transitions need not be considered. The stable states of the protonated water trimer are isomers which interconvert by proton transfer and oxygen ring rearrangement. We find that an order parameter which describes only bonding of the excess proton fails to discriminate sufficiently between these stable states. Rather, as discussed in Section III, a successful characterization is obtained by considering the geometry of the oxygen ring.

Path sampling for transitions between these stable states is discussed in Section IV, and rate constant calculations are presented in Section V. The transition path sampling reveals two separate classes of trajectories connecting the stable states each with its own transition state region. The two transition state regions are separated by a high potential energy barrier. Both classes of trajectories involve a collective cluster rearrangement dominated by motion of the "solvating" water molecule—the molecule not directly involved in the proton transfer. Indeed, we find that a coordinate describing the motion of this "solvating" molecule serves very well as a reaction coordinate for the proton transfer. The potential experienced by the transferring proton shifts as the solvating water moves from one side of the cluster to the other and exhibits no bistability. In this sense the transition dynamics in this model system are qualitatively similar to the dynamics of excess proton transport found in bulk water by *ab initio* molecular dynamics.[5,6] Namely, the proton moves from one water to another guided by rearrangement of local solvation structures rather than by chemical bond distortion. Remarkably, this paradigm applies even to the simplest water cluster in which activated proton transfer is possible.

II Transition path sampling

A Stable states

The efficiency of the path sampling method derives in part from the fact that stable states act as basins of attraction. Displacements of an existing path are clearly more likely to produce acceptable transition paths if initial and final configurations are constrained to lie in attracting rather than repelling regions of phase space. Successful application of the

method consequently requires that the order parameter used to characterize stable states distinguishes between the two basins of attraction. If no range of the order parameter unambiguously specifies a single stable state, most "transition" paths obtained will contain only fluctuations within one stable region rather than the desired transitions to a neighboring stable region. Typically, stable state distributions which do not overlap indicate that an order parameter is sufficiently discriminating. It should be emphasized that this criterion for a useful order parameter does not require that a reaction coordinate is known *a priori*. Transition dynamics may be nearly orthogonal to a discriminating order parameter.

B Pathways and transition states

Generating an initial transition path is one of the significant steps in applying path sampling methods to complex systems. When dynamics cannot be run sufficiently long to observe a single transition, one must attempt to anneal high-temperature paths or initiate trajectories from an artificial transition state-like configuration. One then uses the sampling procedure to relax from what may be an unlikely pathway. Following sufficient equilibration, trajectories may be examined to determine common qualitative aspects of the transition.

For quantitative analysis of transition dynamics, it is useful to define an ensemble of transition states. We consider a configuration to be a transition state if the two stable states are dynamically accessible from the configuration in equal proportions. A collection of such configurations is more meaningful for a complex system at finite temperature than a small set of saddle point configurations. Distributions within the transition state ensemble reveal the degree of dispersion of transition dynamics and allow identification of the true reaction coordinate.

C Correct sampling

In order to generate a proper ensemble of transition paths, it is sufficient that a sampling algorithm satisfy the Monte Carlo detailed balance criterion,

$$P_{\mathrm{gen}}(\mathrm{old}\rightarrow\mathrm{new})P_{\mathrm{acc}}(\mathrm{old}\rightarrow\mathrm{new})F(x_0^{\mathrm{old}}) = P_{\mathrm{gen}}(\mathrm{new}\rightarrow\mathrm{old})P_{\mathrm{acc}}(\mathrm{new}\rightarrow\mathrm{old})F(x_0^{\mathrm{new}}) \quad (1)$$

Here, $P_{\mathrm{gen}}(\mathrm{old}\rightarrow\mathrm{new})$ is the probability of generating a particular new trajectory from an existing one, and $P_{\mathrm{acc}}(\mathrm{old}\rightarrow\mathrm{new})$ is the probability of accepting the new trajectory. $F(x_0)$ is the distribution function of initial conditions x_0. In order to employ a Metropolis method, specified by the acceptance probability

$$P_{\mathrm{acc}}(\mathrm{old}\rightarrow\mathrm{new}) = \min\left[\frac{F(x_0^{\mathrm{new}})}{F(x_0^{\mathrm{old}})}, 1\right] \quad (2)$$

it is necessary that the path generation probability is symmetric, *i.e.*, $P_{\mathrm{gen}}(\mathrm{old}\rightarrow\mathrm{new}) = P_{\mathrm{gen}}(\mathrm{new}\rightarrow\mathrm{old})$.

Our primary method of generating new members of the transition path ensemble is by way of a "shooting" move. A trajectory displacement is achieved by selecting a configuration from an existing path, applying a small displacement to the momenta corresponding to the selected configuration, and integrating forwards and backwards in time. Clearly, the manner in which momentum displacements are chosen must be consistent with the equilibrium distribution of initial conditions (including any physical constraints on the system) and must produce a symmetric path generation probability in order to obey detailed balance. In the Appendix, we consider explicitly a momentum displacement method for a microcanonical ensemble in which the total linear momentum $\boldsymbol{P}$ and the total angular momentum $\boldsymbol{L}$ both vanish. This method may be generalized to treat other linear constraints such as fixed bond lengths or a fixed, non-zero value of the total angular momentum.

D Transition rate constants

In the context of transition path sampling, the time correlation functions which appear in chemical kinetics are isomorphic with simple thermodynamic quantities. Specifically, the correlation $C(t)$ between populations of state A at time zero and state B at time t may be regarded as a ratio of partition functions for two different ensembles of trajectories:

$$C(t) \equiv \frac{\langle h_A(x_0)h_B(x_t)\rangle}{\langle h_A(x_0)\rangle} \quad (3)$$

$$= \frac{Q_{AB}}{Q_A} \quad (4)$$

Here, $h_A(x)$ and $h_B(x)$ are unity if the configuration x belongs to state A or B, respectively, and vanish otherwise. Angled brackets denote equilibrium averages over initial configurations x_0. The partition function Q_{AB} describes an ensemble of trajectories which begin in state A and end in state B. Similarly, the partition function Q_A describes an ensemble in which the endpoint is unconstrained. This ratio of partition functions may therefore be interpreted in terms of the reversible work $w_{AB}(t)$ required to confine the endpoint of an ensemble of trajectories of length t to stable state B given that the initial point lies in state A,

$$C(t) = \mathrm{e}^{-w_{AB}(t)} \quad (5)$$

In order to compute a transition rate constant k_{AB} it is sufficient to determine the time derivative of this correlation function, $k(t) = \dot{C}(t)$. $k(t)$ scales linearly after some transient time with a slope whose value is k_{AB}.

For computational convenience we divide the confinement free energy $w_{AB}(t)$ into two parts,

$$w_{AB}(t) = w_{AB}(t') + \Delta w(t; t') \quad (6)$$

Here, $\Delta w(t; t')$ is the reversible work required to change the trajectory length from an arbitrary time t' to t. This quantity is easily calculated in a single path sampling simulation, whereas the total confinement free energy $w_{AB}(t')$ requires a more costly thermodynamic integration. The reactive flux $k(t)$ may then be computed as

$$k(t) = \mathrm{e}^{-w_{AB}(t')}\nu(t; t') \quad (7)$$

where $\nu(t; t')$ is defined as in ref. 7:

$$\nu(t; t') = -\mathrm{e}^{-\Delta w(t; t')}\frac{\mathrm{d}}{\mathrm{d}t}\Delta w(t; t') \quad (8)$$

This factorization not only improves computational efficiency (as one needs to compute the total confinement free energy for a single trajectory length t'), but also allows a straightforward comparison with traditional reactive flux theory.[9] For adjoining stable states (*i.e.*, in terms of some coordinate q, state A is defined by $q < 0$ and state B by $q > 0$) $\nu(t; t')$ is simply related to the transmission coefficient $\kappa(t)$ of chemical kinetics:

$$\frac{\nu(t; t')}{\nu(0, t')} = \kappa(t) \equiv \frac{\langle \dot{q}\delta(q)\theta[q(t)]\rangle}{\frac{1}{2}\langle|\dot{q}|\delta(q)\rangle} \quad (9)$$

$\kappa(t)$ describes deviations from transition state theory due to dynamical recrossings of the surface $q = 0$. Quantities directly accessible in path sampling simulations may therefore be used to gauge the effects of finite-temperature dynamics upon kinetics.

III Stable states of the protonated water trimer

Ab initio studies at varying levels of accuracy agree that the minimum energy configuration of the protonated trimer is one in which the extra proton is bound to a central water molecule.[3,11] The remaining neutral water molecules stabilize the

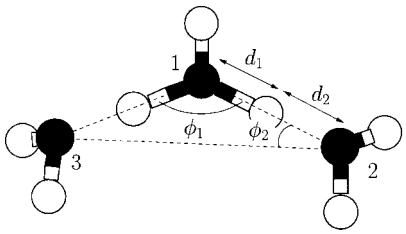

Fig. 1 Minimum energy configuration for the protonated water trimer in the Stillinger–David model potential. The excess proton is bound to water molecule 1 at the center. The terminal water molecules, numbered 2 and 3, accept hydrogen bonds from molecule 1. In order to describe the cluster isomerization, we define the structural quantities d_1, d_2 (measuring the distance from oxygen atoms to the transferring proton), and ϕ_1, ϕ_2 (measuring oxygen ring angles).

excess charge by accepting hydrogen bonds from the central hydronium ion. The Stillinger–David model accurately predicts the qualitative aspects of this stable state. The minimum energy configuration, determined by conjugate gradient quenching, is shown in Fig. 1. We report all other energies relative to this minimum.

The equilibrium configuration is quite stable to dissociation and rearrangement. Of all possible binary decomposition products, the most stable is found to be $H_5O_2^+ + H_2O$ with a dissociation threshold energy of $E = 22.29$ kcal mol^{-1}. In the present study, we consider cluster energies in the range 12–21 kcal mol^{-1} above that of the cluster's minimum energy, coinciding with temperatures between 250 and 440 K, and well below the dissociation threshold. Long equilibrium dynamics simulations (20 ns) at $E = 15.34$ kcal mol^{-1} above the energy minimum yield only fluctuations about the minimum energy structure and rotational exchange of protons on a terminal water molecule. Other cluster rearrangements and bond-breaking processes occur with very long characteristic times.

Equivalence of the three oxygen atoms in the cluster ensures that three degenerate stable states exist. In each state, a different oxygen atom lies at the center of the cluster and possesses the excess proton. We have chosen the geometry in Fig. 1 as the initial stable state (A) and a geometry with molecule 2 at the center as the final state (B). The equilibrium structure suggests two simple order parameters describing the bonding and coarse geometry of the cluster, respectively. The difference in chemical bonding between the stable states is well-described by distances of the relevant oxygen atoms to the excess proton, $\Delta r \equiv d_1 - d_2$. (See Fig. 1 for definitions of bond distances d and ring angles ϕ). Collective cluster rearrangement is more effectively described by a function of the oxygen ring geometry, such as $\Delta\phi \equiv \phi_1 - \phi_2$.

A series of simple simulations demonstrate that Δr is in fact a poor choice of order parameter for the transition described above. Starting with the cluster in stable state A, we generate a series of order parameter values Δr_i ranging from typical values in state A to typical values in state B. The system is then allowed to relax for 2.5 ps, subject to each constraint $\Delta r = \Delta r_i$, using a modified RATTLE algorithm.[12] It is found that the oxygen ring geometry remains as in stable state A for each constraint value, *i.e.*, the system does not relax to state B, even for values of Δr characteristic of that state. The bonding order parameter Δr thus fails to discriminate between the stable states. For this reason we use the order parameter $\Delta\phi$ to identify stable states in path sampling simulations. We define state A by $\Delta\phi < -5°$, and state B by $\Delta\phi > 5°$.

IV Proton transfer pathways

We generated an initial proton transfer path by allowing the system to relax from a configuration symmetric with respect to exchange of water molecules 1 and 2. Because the dynamics does not break symmetry, a local minimum in the constrained space $\Delta\phi = 0°$ is obtained by simulated annealing. Initiating trajectories from the relaxed configuration results in successful transition paths.

Beginning with such an initial path, we sampled the transition path ensemble for a variety of energies. A series of snapshots along a typical path at $E = 15$ kcal mol^{-1} is shown in Fig. 2. (E refers to the energy of the cluster relative to its minimum potential energy.) Transfer of a proton from molecule 1 to molecule 2 requires a substantial rearrangement of the cluster. During the transition, water molecule 3, which initially accepts a hydrogen bond from molecule 1, moves to the opposite side of the cluster, and the excess proton is transferred from molecule 1 to molecule 2. Because the barrier to isomerization is a significant fraction of the available energy, the dynamics slow considerably as the system approaches the saddle point. The system slowly passes through a transition state region, then accelerates and completes the transition in about 300 fs. In the new stable state molecule 3 accepts a hydrogen bond from molecule 2.

We have observed qualitatively different pathways in our simulations. While the initial path was created using the saddle point configuration shown in Fig. 3(a) ($E = 14.18$ kcal mol^{-1}), the energetically more favorable saddle point configuration shown in Fig. 3(b) ($E = 11.73$ kcal mol^{-1}) was found automatically by the sampling procedure. This second saddle point is apparently stabilized by an antiparallel alignment of

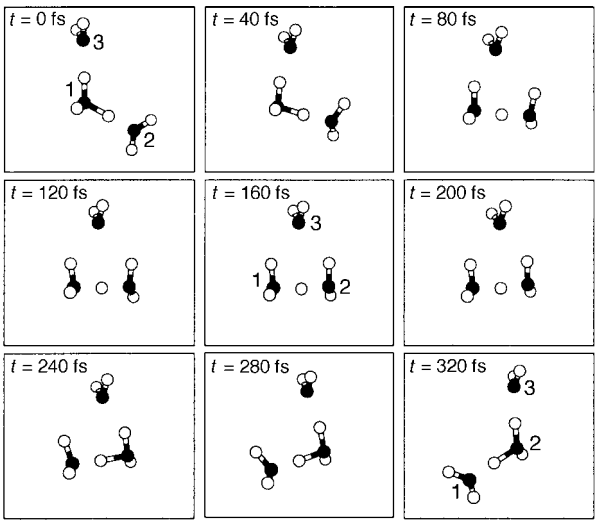

Fig. 2 Snapshots of the protonated water trimer along a transition trajectory. During the transition a proton is transferred from water molecule 1 to water molecule 2 as molecule 3 moves from the left to the right side of the cluster. Consecutive configurations are separated by 40 fs.

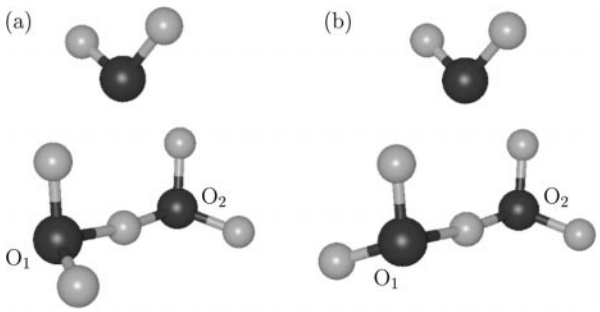

Fig. 3 The two relevant saddle points found using the path sampling procedure with energies $E = 14.18$ kcal mol^{-1} (a) and $E = 11.73$ kcal mol^{-1} (b). In the higher energy transition state (a) the out-of-plane hydrogen atoms of water molecules 1 and 2 lie on the same side of the oxygen plane. In the lower energy transition state (b) these hydrogens lie on opposite sides of the plane, so that the dipoles of water molecules 1 and 2 are antiparallel.

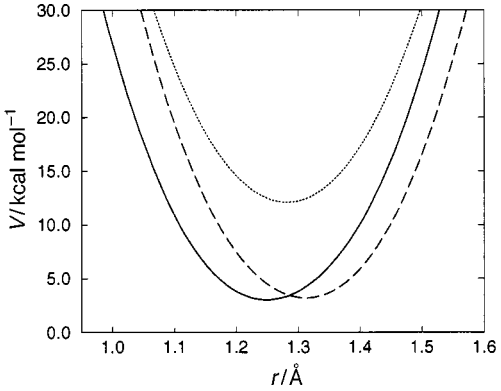

Fig. 4 Instantaneous proton potentials as a function of the O_1–H distance r along a line parallel to the O_1–O_2 line. The solid and broken lines show the proton potentials in the stable states. The dotted line shows the potential experienced by the transferring proton at the transition state. Throughout the transition the proton potential is monostable.

the dipoles of molecules 1 and 2. Rotating water molecule 2 about its hydrogen bond to molecule 3, one finds that the lower transition state is separated from the higher transition state by a barrier of approximately 6 kcal mol^{-1}. The path sampling method generates both pathways even though they are separated by a high potential energy barrier.

In order to determine the driving mechanism for these dynamics, we collected approximately 1000 transition states for an energy of $E = 15.34$ kcal mol^{-1} (near ambient temperature). Because kinetic energies are small near transition states at this energy, dispersion of configurations in the transition state ensemble is limited. Only small fluctuations about the symmetric structure in Fig. 3(b) are observed. Narrow distributions of the structural order parameters Δr (with variance 3.3×10^{-2} Å) and $\Delta\phi$ (with variance 1.0°) in the transition state ensemble reflect this fact.

By aligning transition paths according to the times at which they pass through transition states, we may critically assess the quality of these order parameters as reaction coordinates. Distributions of the time derivatives $\Delta\dot{r}$ and $\Delta\dot{\phi}$ at the transition state indicate the extent to which each order parameter changes monotonically during the transition. The distribution of $\Delta\dot{r}$ is nearly symmetric about $\Delta\dot{r} = 0$ (with mean -1.3×10^{-4} Å fs^{-1} and variance 1.2×10^{-2} Å fs^{-1}), implying that the dynamics of the transferring proton are primarily high-frequency fluctuations within a slowly moving potential well. By contrast, the distribution of $\Delta\dot{\phi}$ is strongly asymmetric about $\Delta\dot{\phi} = 0$ (with mean $-0.11°$ fs^{-1} and variance $0.10°$ fs^{-1}), suggesting that a consistent directional motion of the non-participating water is responsible for the transition. It is indeed the oxygen ring rearrangement which drives the dynamics of isomerization and proton transfer.

This understanding is confirmed both by an eigenvector analysis of the minimum-energy transition state and by measurement of the dynamical potential experienced by the transferring proton. Upon diagonalizing the mass-weighted Hessian matrix for the transition state, one finds a single negative eigenvalue, indicating a single unstable mode. The eigenvector for this mode corresponds to a collective motion which is predominantly in the direction of $\Delta\phi$ with Δr fixed. Within the context of transition state theory, this unstable mode is the optimal reaction coordinate for barrier crossing. Since we observe only a small percentage of transition paths which recross the phase-space dividing surface $\Delta\phi = 0°$ (as discussed in the next section) this non-dynamical perspective should be qualitatively accurate.

A consequence of the rearrangement-driven nature of this process is that the transferring proton experiences a monostable potential throughout the transition. We construct a reduced-dimension visualization of the instantaneous proton potential by computing energies for a series of proton displacements parallel to the O_1–O_2 line. Over the course of a typical transition, the minimum of the proton shifts systematically towards the accepting water molecule. The curvature of this well does not change appreciably during the transfer, and at no time does the transferring proton experience a double-well potential (see Fig. 4). Quantum mechanical corrections to rate constants measured using classical proton dynamics are therefore expected to be small.

V Rate constants

Using the path sampling procedure described in Section II and in refs. 7 and 9, we have computed isomerization rate constants $k_{A\to B}$ for a variety of energies corresponding to average temperatures in the range 250–430 K. Each rate constant was computed from simulations consisting of tens of thousands of transition paths. As an example, the correlation function $C(t)$, from which the rate constant is extracted, is plotted in Fig. 5 for an energy $E = 15.34$ kcal mol^{-1}. Characteristic reaction times depend very sensitively on the total energy of the cluster (see Fig. 6). Even at the highest energies, proton transfer in this cluster remains an extremely slow process.

The small number of recrossings observed in our path sampling simulations suggest that the transition rate constant should be accurately predicted by classical RRKM theory.[13]

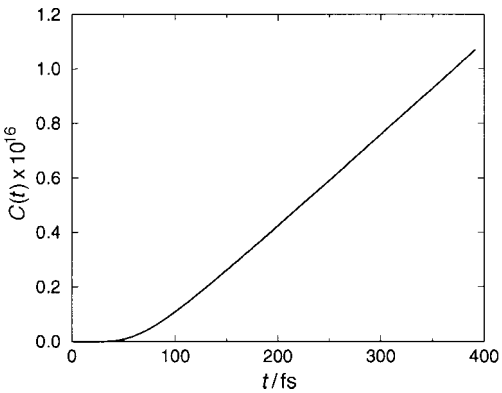

Fig. 5 Time correlation $C(t)$ of stable state populations as a function of time t. After a transient period, $C(t)$ scales linearly with time. The slope in this linear regime corresponds to the reaction rate constant.

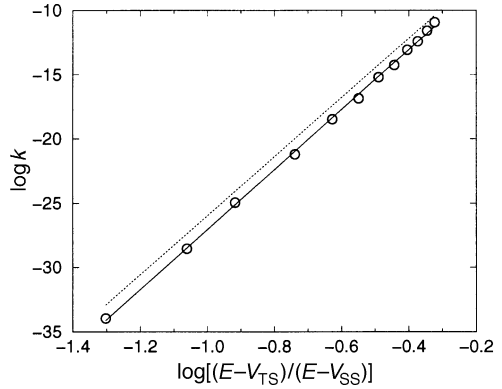

Fig. 6 Logarithm of the reaction rate constant k as a function of the logarithm of the energy ratio $(E - V_{TS})/(E - V_{SS})$. The circles represent simulation results with statistical uncertainties represented by the size of the plotted symbols. The solid line is a linear fit to the simulation results, and the broken line shows the prediction of RRKM theory. The fitted line has slope $s - 1 = 23$, indicating that all degrees of freedom (with the exception of three translational and three rotational degrees of freedom) are coupled to the reaction. A hydrogen mass of 2 u was used in all calculations.

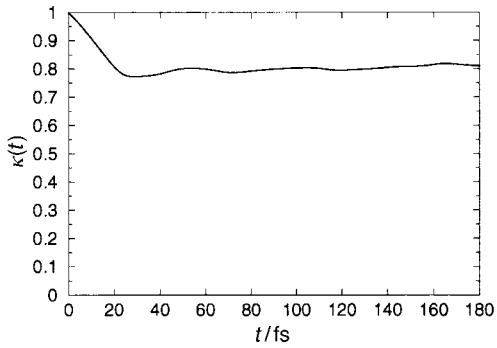

Fig. 7 Transmission coefficient $\kappa(t)$ obtained from reactive flux calculations for a dividing surface defined by $\Delta\phi = 0$ for a total energy $E = 15.34$ kcal mol^{-1}. Following transient behavior in the first 50 fs, $\kappa(t)$ reaches a plateau with value ~ 0.75.

In this approximation the system is treated as a set of harmonic oscillators both in the stable state and at the saddle point. Under the assumption that every trajectory reaching the transition state is a reactive trajectory RRKM theory yields the following expression for the rate constant:

$$k_{\mathrm{RRKM}}(E) = \frac{\prod_{i=1}^{s} \omega_i^{\mathrm{SS}}}{\prod_{i=1}^{s-1} \omega_i^{\mathrm{TS}}} \left(\frac{E - V_{\mathrm{TS}}}{E - V_{\mathrm{SS}}}\right)^{s-1} \tag{10}$$

Here $s = 30 - 6 = 24$ is the total number of degrees of freedom. V_{TS} is the potential energy at the saddle point, and V_{SS} is the potential energy at the stable state energy minimum. ω_i^{SS} and ω_i^{TS} are the vibrational frequencies of the stable modes at the stable state and the transition state, respectively.

The predictions of RRKM theory compare well with our simulation measurements. The logarithm of the transition rate constant as a function of $\log[(E - V_{\mathrm{TS}})/(E - V_{\mathrm{SS}})]$ is plotted in Fig. 6. A linear fit to the simulation data results yields a slope of $s - 1 \approx 23$. This agreement with RRKM theory indicates that all degrees of freedom (with the exception of global rotations and translations) are coupled to the transition. RRKM estimates of the transition rate constant and the simulation results differ consistently by a factor of ~ 15. This discrepancy could in principle arise both from dynamical recrossings of the transition state and from anharmonicity of the potential surface. However, few recrossings are observed. For a dividing surface defined by $\Delta\phi = 0°$, a transmission coefficient κ greater than 70% (see Fig. 7) is obtained. The deviation of RRKM predictions must therefore result from important nonlinearities of the potential near the energy minimum. At energies large enough to observe proton transfer, RRKM theory underestimates the stable state partition function and consequently overestimates the transition rate constant.

Acknowledgements

This work was initiated with support from the National Science Foundation and completed with support from the Department of Energy through the Chemical Sciences Division of Lawrence Berkeley National Laboratory. C.D. is a Schrödinger Fellow of the Austrian Fonds zur Förderung der wissenschaftlichen Forschung (grants J1302-PHY and J1548-PHY). P.L.G. is a National Science Foundation Predoctoral Fellow and was a Berkeley Fellow for part of this work.

Appendix

For systems in which the masses of all particles are not identical, it is most convenient to work in mass-weighted coordinates,

$$\boldsymbol{q}_i \equiv \sqrt{m_i}\,\boldsymbol{r}_i$$
$$\boldsymbol{w}_i \equiv \dot{\boldsymbol{q}}_i \tag{11}$$

where $\boldsymbol{r}_i$ is the position vector of the ith particle. In this coordinate representation, the constant energy constraint,

$$\mathscr{H} = K + V(\boldsymbol{q}) \tag{12}$$

defines a hypersphere centered at the origin of the high-dimensional $\boldsymbol{w}$-space

$$\sum_i |\boldsymbol{w}_i|^2 = 2[\mathscr{H} - V(\boldsymbol{q})] \tag{13}$$

The remaining linear constraints,

$$\boldsymbol{P} = \sum_i \sqrt{m_i}\,\boldsymbol{w}_i = 0 \tag{14}$$

$$\boldsymbol{L} = \sum_i \boldsymbol{q}_i \times \boldsymbol{w}_i = 0 \tag{15}$$

define planes in this same space which intersect the constant-energy hypersphere. The domain of intersection defines a hypersphere $\Omega(\boldsymbol{q})$ of lower dimension centered at the origin. $\Omega(\boldsymbol{q})$ is the subspace of possible momenta for a given configuration $\boldsymbol{q}$. A particular choice of momenta is defined by a vector $\boldsymbol{w}$ in the plane of intersection. In the ensemble of interest, $\boldsymbol{w}$ is distributed evenly on the hypersphere $\Omega(\boldsymbol{q})$. A correct scheme for sampling this distribution follows.

One first selects a displacement $\delta\boldsymbol{w}_i^{(0)}$ for each particle at random from a Gaussian distribution. The set of $\delta\boldsymbol{w}_i^{(0)}$ may be pictured as a vector $\delta\boldsymbol{w}^{(0)}$ in the high-dimensional $\boldsymbol{w}$-space. Constraints are imposed by subtracting components of $\delta\boldsymbol{w}^{(0)}$ orthogonal to the set of constraints. A normal vector for the jth constraint σ_j is provided by the gradient with respect to $\boldsymbol{w}$:

$$\boldsymbol{N}_j = \nabla_{\boldsymbol{w}}\sigma_j \tag{16}$$

In this case σ_j may be any of the components of $\boldsymbol{P}$ and $\boldsymbol{L}$. Because the linear and angular momentum constraints are not mutually orthogonal, one must first compute an orthonormal set of vectors $\hat{\boldsymbol{n}}_j$ spanning the same space as the $\boldsymbol{N}_j$ before projecting out components of $\delta\boldsymbol{w}^{(0)}$. A Gram–Schmidt procedure is sufficient for this purpose. Once the basis vectors $\hat{\boldsymbol{n}}_j$ have been constructed, a random orientational displacement $\delta\boldsymbol{w}^{(0)}$ in the plane of $\Omega(\boldsymbol{q})$ may be obtained by sequentially removing the components of $\delta\boldsymbol{w}^{(0)}$ along each $\hat{\boldsymbol{n}}_j$:

$$\delta\boldsymbol{w} = \delta\boldsymbol{w}^{(0)} - \sum_j (\delta\boldsymbol{w}^{(0)} \cdot \hat{\boldsymbol{n}}_j)\hat{\boldsymbol{n}}_j \tag{17}$$

One then adds the displacement $\delta\boldsymbol{w}$ to the original mass-weighted momenta and rescales to obtain the appropriate total energy:

$$\boldsymbol{w}' = \alpha[\boldsymbol{w} + \delta\boldsymbol{w}] \tag{18}$$

The rescaling factor α is given by

$$\alpha = \left[\frac{\sum_i |\boldsymbol{w}_i|^2}{\sum_i |\boldsymbol{w}_i + \delta\boldsymbol{w}_i|^2}\right]^{1/2} \tag{19}$$

This process guarantees that the probability of selecting a new set of mass-weighted momenta $\boldsymbol{w}'$ from an existing set $\boldsymbol{w}$ is equal to the probability of selecting $\boldsymbol{w}$ from $\boldsymbol{w}'$, so that detailed balance is satisfied explicitly.

References

1 M. Parrinello, *Solid State Commun.*, 1997, **102**, 107.
2 F. H. Stillinger and C. W. David, *J. Chem. Phys.*, 1978, **69**, 1473.
3 U. W. Schmitt and G. A. Voth, *J. Phys. Chem.*, 1998, **102**, 5547.

4 R. Vuilleumier and D. Borgis, *Chem. Phys. Lett*., 1998, **284**, 71.
5 M. Tuckerman, K. Laasonen, M. Sprik and M. Parrinello, *J. Chem. Phys*., 1995, **103**, 150.
6 M. Tuckerman, K. Laasonen, M. Sprik and M. Parrinello, *J. Phys. Chem*., 1995, **99**, 5749.
7 P. G. Bolhuis, C. Dellago and D. Chandler, *Faraday Discuss*., 1998, **110**, 421.
8 C. Dellago, P. G. Bolhuis, F. S. Csajka and D. Chandler, *J. Chem. Phys*., 1998, **108**, 1964.
9 C. Dellago, P. G. Bolhuis and D. Chandler, *J. Chem. Phys*., 1999, **110**, in press.
10 P. L. Geissler, C. Dellago, D. Chandler, J. Hutter and M. Parrinello, in preparation.
11 E. P. F. Lee and J. M. Dyke, *Mol. Phys*., 1991, **73**, 375.
12 H. C. Andersen, *J. Comput. Phys*., 1982, **52**, 24.
13 L. S. Kassel, *J. Phys. Chem*., 1928, **32**, 225; O. K. Rice and H. C. Ramsperger, *J. Am. Chem. Soc*., 1927, **49**, 1617; O. K. Rice and H. C. Ramsperger, *J. Am. Chem. Soc*., 1927, **50**, 617; R. Marcus and O. K. Rice, *J. Phys. Colloid Chem*., 1951, **55**, 894.

Paper 8/08871C